HiSST: 3rd International Conference on
High-Speed Vehicle Science Technology
14 -19 April 2024, Busan, Korea

Experimental aeroshape characterization of an Inflatable Heat Shield re-entry vehicle in the EFESTO-2 project.

J.Zhai, T.Gawehn, A. Guelhan[1], Y.Prevereaud, Y.Dauvois[2], G.Guidotti[3], G.Governale[4]

Abstract

Inflatable Heat Shields (IHS) represent a breakthrough solution that supports the realization of innovative re-entry space missions by significantly increasing payload capability and enhancing space systems' recovery potential. To make this solution operational, several key technologies must be matured to an appropriate level. Within the scope of the EFESTO-2 project, structural and aerodynamic ground tests have been planned to advance our understanding of this unique inflatable aerodynamic decelerator system. To achieve this objective, a numerical study is conducted to simulate the maximum expected deformation level of the heat shield during re-entry. Subsequently, both nondeformed and deformed shapes of the heat shield are tested in the H2K and TMK wind tunnels. Following this, post-test numerical analysis will be conducted.
This paper presents the efforts and achievements pertaining to the aerodynamic investigation of aero-shapes in the hypersonic wind tunnel H2K and the supersonic wind tunnel TMK. It encompasses aspects such as the specification of wind tunnel models, test conditions, measurement techniques, and the evaluation of test results.

Keywords: *inflatable heat shields, hypersonic re-entry aerodynamics and aerothermodynamics, wind-tunnel testing, numerical rebuilding, fluid-structure interaction*

Nomenclature

Angle of Attack (AoA)
Computational Fluid Dynamic (CFD)
Finite Element Method (FEM)
Fluid Structure Interaction Loop (FSI)
Inflatable Heat Shield (IHS)
Flexible TPS (F-TPS)
Inflatable Structure (IS)
Thermal Protection System (TPS)
Technology Readiness Level (TRL)
Wind Tunnel Test (WTT)
Natural Transition (NT)
Tripped Transition (TT)

1. EFESTO-2 project set-up

Inflatable Heat Shields (IHS) are considered as a breakthrough solution to support realization of innovative re-entry space missions as increasing significantly payload capability and space systems' recovery. For this solution to become operational, a number of key technologies must be matured to an appropriate readiness level and that's what is being done in Europe through the projects EFESTO (Guidotti, 2022) (Governale, 2022) (Gardi, 2022) (Schleutker, 2022) and EFESTO-2, respectively under the programs H2020 (grant nr.821801) and HORIZON EUROPE (grant Nr. 1010811041). EFESTO-2 project is managed by a European consortium coordinated by Deimos Space (ES), that includes ONERA

[1] *German Aerospace Center (DLR), Supersonic and Hypersonic Technologies, Köln, Germany*
[2] *Office National d'Etudes et de Recherches Aerospatiales (ONERA), Toulouse, France*
[3] *Deimos Space S.L.U, Tres Cantos 28760, Spain*
[4] *Politecnico di Torino, Department of Mechanical and Aerospace Engineering, Turin – Italy*

Copyright © 2024 by author(s)

(FR), DLR (DE), CIRA (IT), POLITO (IT), DEIMOS ENGHENARIA (PT), and PANGAIA-GRADO-ZERO (IT). This project is run through four main macro-tasks as follows: a business case analysis, a reference mission and system engineering, an extensive ground testing and eventually near-future activities identification.

Based on a Business Case analysis, a reference study-case for a baseline application (see Fig. 1) is selected and then a design loop is executed to define the mission envelope and to derive the system mechanical and thermal sizing of a re-entry vehicle with an integrated inflatable heat shield (Guidotti, 2023) (Dietlein, 2023) (Prevereaud, 2024).

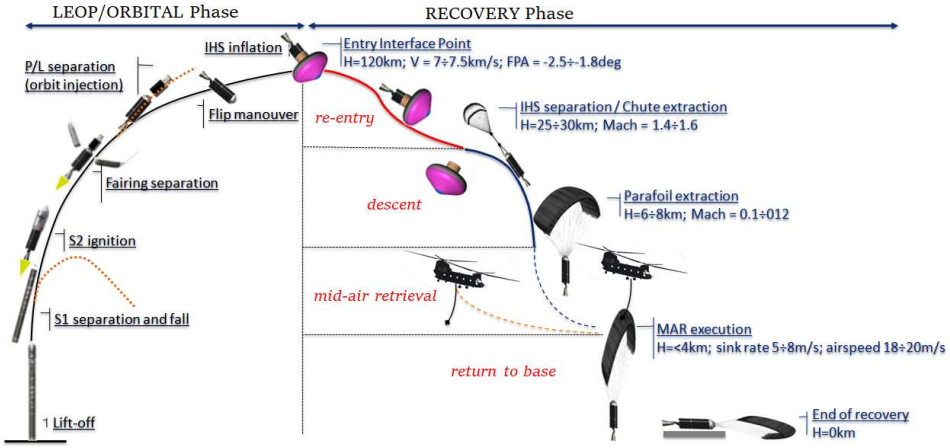

Fig. 1 EFESTO-2 ConOps and system configuration

In the EFESTO-2 project, a particular focus is dedicated to aeroshape investigation, in terms of aerodynamics and aerothermodynamics, including numerical and experimental efforts. The objective is to evaluate the influence of the heat-shield deformation on the aerodynamic coefficients.

To address this goal, a numerical study is carried out to determine the maximum expected deformation level of the heat shield during re-entry and to quantify the influence of this deformation on the aerodynamic coefficients. Based on these data, nondeformed and deformed shape models are designed and tested in the DLR H2K and TMK wind tunnels for the evaluation of static and dynamic stability. Then, a numerical rebuilding of the wind-tunnel tests is done to calibrate numerical models, to update and consolidate the aerodynamic database and enhance the flying quality assessment. This paper presents the efforts and achievements pertaining to the experimental investigation of the aeroshapes in the hypersonic wind tunnel H2K and the supersonic wind tunnel TMK. It encompasses aspects such as the specification of wind tunnel models, test conditions, measurement techniques, and the evaluation of test results.

2. Experimental aerodynamic characterization of the IHS

The aeroshape characterization of the EFESTO-2 IHS encompasses the whole loop from numerical simulation with CFD, to experimental investigation through wind-tunnel testing, and finally with cross-check between numerical and experimental results to update the aero-database set (see Fig. 2).

The process includes the following steps: 1) Aerodynamic and aerothermodynamic analysis of the reference nondeformed shape; 2) Fluid structure interaction analysis to define the maximum level of deformation; 3) Wind-tunnel tests; 4) WTT-CFD cross-check to evaluate uncertainties associated to numerical simulation and to report these uncertainties into the aerodynamic database to consolidate the mission and system design.

Copyright © 2024 by author(s)

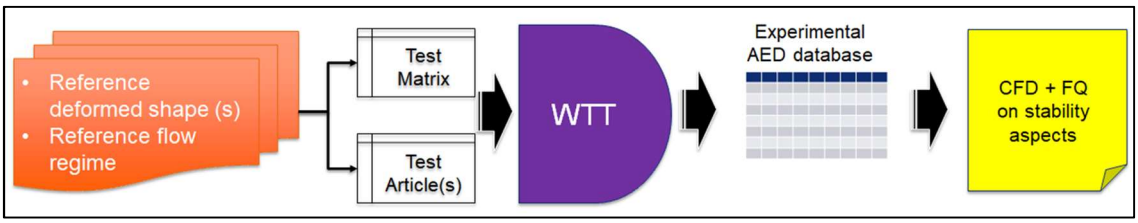

Fig. 2 Aerodynamic experimental and numerical investigation

Of significant importance in the frame of the project is the execution of a wind-tunnel test campaign designed to investigate the aerodynamics and flying qualities of capsule-like bodies in both deformed and nondeformed conditions. Building upon the results obtained in step 2, two DLR-Cologne facilities, the Hypersonic Wind Tunnel Cologne (H2K) and the Trisonic Wind Tunnel Cologne (TMK), have been engaged for this purpose. The operational capabilities of the facilities, as they relate to the reference trajectory of EFFESO-2, are depicted in Fig. 3.

In H2K, the hypersonic phase is replicated for static tests using the deformed aeroshape at Mach numbers of 7 and 5.3. Meanwhile, in TMK, the supersonic phase is replicated for both static and dynamic tests using the nondeformed aeroshape across the Mach range from 4 to 1.4.

For WTT strategy, it is optimal to replicate the dynamic pressure or Reynolds number using the deformed aeroshape in H2K and to replicate the Reynolds number using the nondeformed aeroshape in TMK.

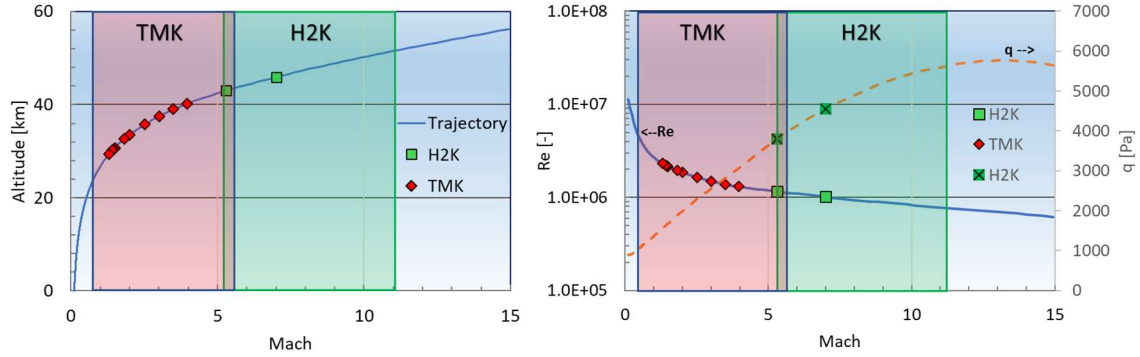

Fig. 3 Trajectory and test conditions

3. EFESTO-2 in hypersonic phase - H2K

3.1. Experimental setup

Hypersonic wind tunnel Cologne (H2K)

The H2K facility of DLR (shown in Fig. 4) is a blow-down wind tunnel. In this setup, pressurized air, with pressures of up to 55 bar, is introduced into the tunnel. To prevent condensation and facilitate operation at various stagnation temperatures, electrical heaters with a heating capacity of up to 5 MW are used to heat the air, that is first blown into the atmosphere during the heating process until the desired stationary stagnation temperature is achieved. Then, a 3/2 valve is activated to allow the air to flow through a contoured axisymmetric nozzle, which has an exit diameter of 600 mm, before entering a free-jet test section. Subsequently, the exhaust flow is directed into a vacuum sphere. Thanks to the independent control of pressure and temperature, adjustments to the Reynolds number and dynamic pressure can be made separately (Niezgodka, 2000).

Copyright © 2024 by author(s)

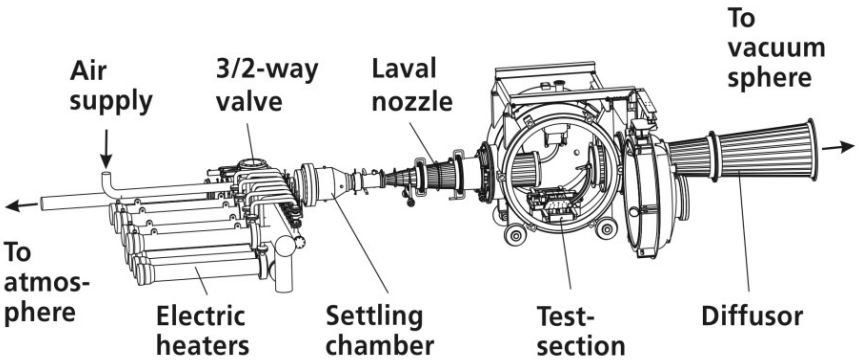

Fig. 4 Schematic drawing of H2K

Test durations typically last around 30 seconds, depending on the specific test conditions. By exchanging the wind tunnel nozzle, various Mach numbers such as 5.3, 6.0, 7.0, 8.7, and 11.2 can be achieved. The unit Reynolds number operating range is between 2.5 and 20 million m^{-1}, depending on the total pressure and total temperature.

3.2. Wind tunnel model

Considering the allowable tunnel blockage, balance loads, and the required Reynolds numbers, a model scale factor of 0.02 is defined for testing in H2K. According to results of the Fluid-Structure Interaction loop performed, the deformed aeroshape, as illustrated in Fig. 5 on the left, is tested in H2K. The deformed aeroshape has a small dent on the conical side wall, and the toroidal cross-section is no more circular.

To prepare for the wind tunnel test campaign, it is imperative to understand the loads acting on the model. These loads are crucial for selecting an appropriate wind tunnel balance and designing a calibration scheme to achieve optimal accuracy. Additionally, they are instrumental in optimizing the model's structure. To this end, a numerical simulation was conducted for the H2K at Mach 7 and 5.3 under high Reynolds number flow conditions. The mesh was generated using the commercial mesh generator CENTAUR. The flow solver TAU, developed by DLR (Langer, 2018), was employed for the simulation. TAU applies the finite volume method to solve the Navier–Stokes equations. In this simulation, the one equation Spalart–Allmaras turbulent model (SAO) was utilized.

Fig. 5, left gives the dimensions of the deformed wind tunnel model. In the middle, the sectional view of the optimized wind tunnel model design is presented. It features a shell structure meticulously designed to minimize weight and consists of three main components: the central body, along with the front and rear heat shields. The front shield and the central body are manufactured of Ramax, a type of high-strength, precipitation-hardened stainless steel. The back shield is made of a high strength aluminium alloy (EN AW 7022). An FEM simulation indicates that any potential gaps and steps between model parts under aerodynamic loads are negligible. The balance is mounted within the central section. On the right side of Fig. 5, the final model mounted on the sting is presented.

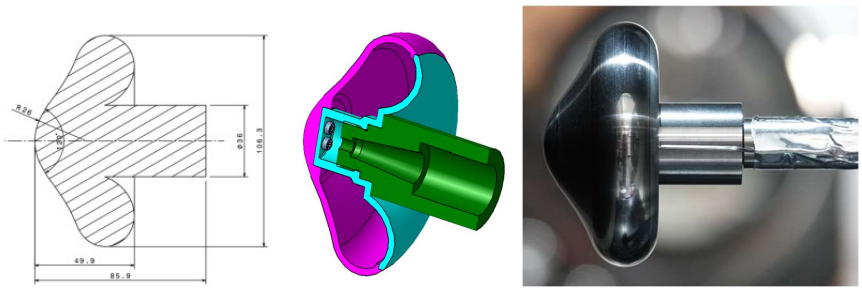

Fig. 5 The wind tunnel model of the deformed aeroshape for H2K

Copyright © 2024 by author(s)

3.3. Static aerodynamic measurements

Aerodynamic coefficients are determined utilizing the internal six-component strain gage balance DLR – 8902. The axial component Fx is positioned centrally within the balance, ensuring minimal interference from other components. Four moment-measuring elements, situated at the balance's ends, are used to determine the longitudinal components Fz and My, as well as the lateral components Fy and Mz. In addition, the rolling moment Mx is measured by sensing the shear strain at the model-side of the balance.

The outer diameter of the balance measures 18mm. Prior to the test, the balance underwent calibration, with calibration points optimized based on the estimated loads from CFD simulation. Table 1 outlines the load range, maximum error, and the 95% uncertainty associated with each component. The maximum error and uncertainty values were derived from the calibration data. To calculate the uncertainty of the coefficients, the maximum error of the balance is utilized.

Table 1 Technical data of balance DLR-8902

Component	Load range	Max. error	95% Uncertainty
Fx [N]	500	0.37	0.17
Fy [N]	250	0.18	0.06
Fz [N]	400	0.07	0.05
Mx [Nm]	25	0.009	0.007
My [Nm]	12.5	0.003	0.002
Mz [Nm]	2	0.009	0.003

Fig. 6 illustrates the test setup, wherein the model is securely affixed to the balance via the conical connection inside the central body. Subsequently, the balance is attached via a second conical connection to the sting. To shield the balance from the tunnel flow it is encased with a protective tube. Fig. 7 shows the model mounted in the test section of H2K.

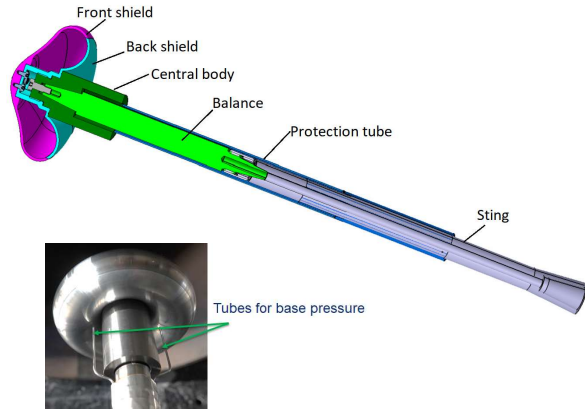

Fig. 6 Test setup

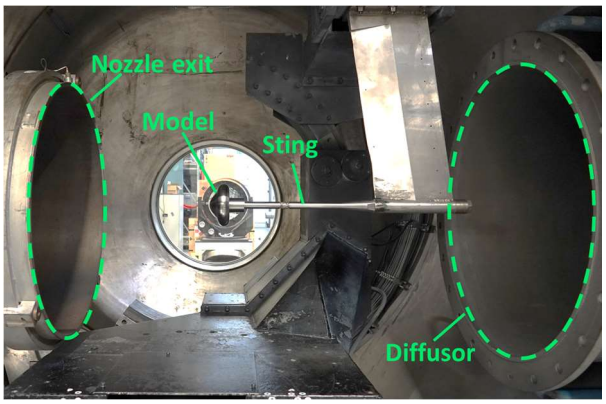

Fig. 7 Model in the test section of H2K

The base pressure downstream of the model is measured using two Kulite absolute sensors. These sensors are directly connected to two tubes (with an outer diameter of 1.6 mm, an inner diameter of 1mm and a length of 50 mm) that are fixed on the sting, as illustrated in Fig. 6. This setup helps to minimize the delay in the pressure measurements.

An FEM simulation of the model, balance, and sting system reveals that the smallest natural frequency amounts to 28 Hz. Its mode shape corresponds to an oscillation in the lateral plane.

Copyright © 2024 by author(s)

Taking these factors into account, the pressure, temperature, angle of attack and balance signals are recorded with an acquisition rate of 50Hz. Subsequently, the coefficients are smoothed using a Gaussian filter with a window length of 25 and a standard deviation of 10. This corresponds with a cut-off frequency of 1 Hz.

3.4. Flow visualizations

For flow visualization the Z-type schlieren system depicted in Fig. 8 is employed. A nano-flashlamp with a flash duration of approximately 10ns serves as a point light source (Daub, 2022). A high-speed camera (Fastcam SA-X2) with a resolution of 1024x1024 captures the images at a rate of 50 fps after cutting of certain deflected parts of the light beam using a knife-edge. The camera exposure time is set at 0.1ms. It focuses on the whole flow field. Simultaneously, another camera (PCO) with higher resolution of 1648x1214 focuses on the flow field around the capsule. It captures the images at a rate of 20 fps. Its exposure time is set at 0.031ms. The nano-flashlamp and the two cameras are synchronized with a trigger system.

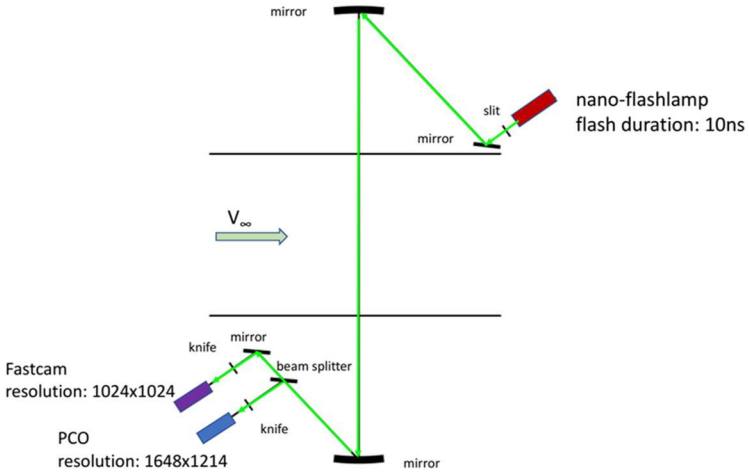

Fig. 8 Schematic of the schlieren system

3.5. Experimental test campaign

As described in section 2, a flow-structure interaction occurs in the hypersonic phase. Therefore, it is of interest to replicate Mach number, Reynolds number, and dynamic pressure in the wind tunnel to investigate the aerodynamic characteristics of the IHS. However, H2K has limitations in simultaneously adjusting both Reynolds number and dynamic pressure within its performance range. Therefore, three distinct conditions are established for both Mach numbers.

In one condition, the trajectory's Reynolds number is replicated, while in the second condition, dynamic pressure is replicated. A third condition is introduced to study potential Reynolds number effects. The test conditions and the trajectory are illustrated in Fig. 9. Of the three conditions, the equivalent Re condition has the highest Reynolds number and dynamic pressure. The equivalent dynamic pressure has the lowest Reynolds number and dynamic pressure. The third condition lies between these two.

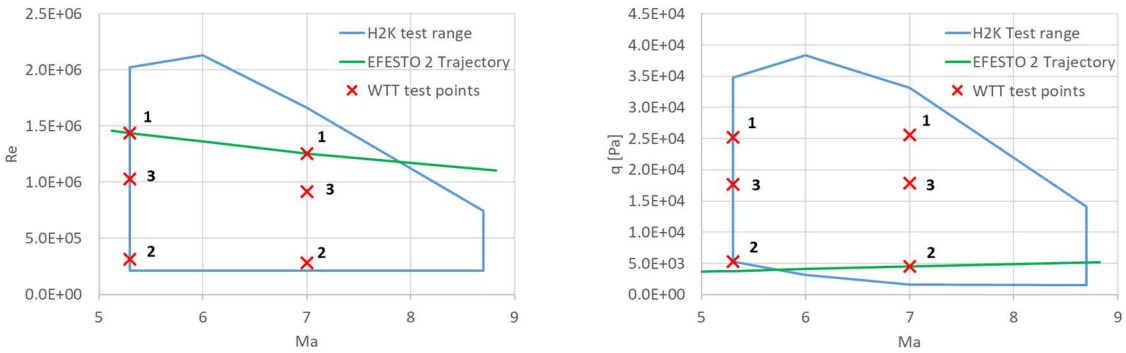

Copyright © 2024 by author(s)

Fig. 9 Test conditions at H2K

Two model conditions are examined: one with a smooth surface to simulate natural transition of the boundary layer (NT), while the other involves coating the model with carborundum to simulate a turbulent boundary layer (trapped transition, TT). In the hypersonic regime, carborundum with a grit size of 400 µm is applied. The entire front surface is coated to prevent relaminarization. The coated model is illustrated in Fig. 10.

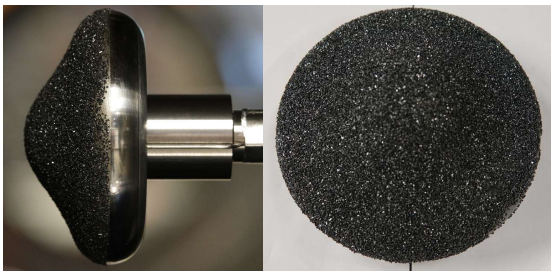

Fig. 10 Model coated with carborundum 400µm for test in H2K

To avoid any potential start-up and shut-down problems, the model is set at an AoA of zero degrees during these phases. Following a short transitional period in the tunnel, data are recorded under constant flow conditions, with AoA sweeping continuously from 0° to -5°, then to 15° and finally back to 0° at a speed of 3°/s.

Schlieren images are captured during the test; however, the cameras do not provide a precise time stamp for each frame. Consequently, correlating the images directly with the measurements is not feasible. To address this issue, the corresponding model's AoA is determined for each individual image during post-processing, utilizing the pattern match technique.

Initially, a template with a known AoA is created, featuring distinguishable features marking the position of the model. For this test, the template comprises the central body and a portion of the back shield of the model. The front shield is excluded due to occasional obscuration behind the bow shockwave. Subsequently, this template is sought in each schlieren image. Upon detection, the AoA is determined. The accuracy of this process is approximately 0.1°.

3.6. Experimental results

The body-fixed coordinate system illustrated in Fig. 11 is utilized for defining the aerodynamic coefficients. Its origin is located at the nose of the IHS and shows the positive direction of axes and AoA. The x-axis aligns with the symmetry axis of IHS and is positive against flow direction. The z-axis is positive downwards. Consequently, the y-axis points positive to the right.

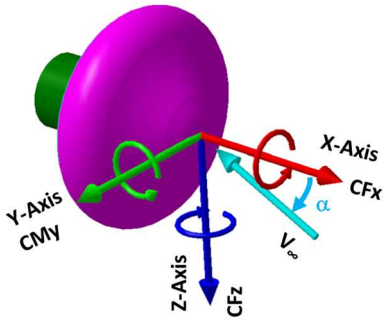

Fig. 11 Aerodynamic coordinate system

Fig. 12 displays the aerodynamic coefficients as a function of AoA for the three test conditions at Mach 7. At this Mach number, it's noted that the axial force coefficient increases in absolute values when the

Copyright © 2024 by author(s)

Reynolds number is decreased. This accounts for the whole investigated angle of attack range from -5° to +15°. In all three cases, the axial force coefficient is roughly constant in the range between -5° and +5° and then decreases in absolute values towards higher AoA. The inverse dependency of the Reynolds number is observed for the base pressure coefficient: Cpb decreases in absolute values when Re is decreased whereby, for the lowest Reynolds number, the value is about zero for small AoAs.
Decreasing the Reynolds number from 1.2 Mio to 0.9 Mio does not influence the normal force and pitching moment coefficient curves, but a further decrease to 0.3 Mio reveals an impact above +5° AoA, where a gradual shift of both curves towards higher absolute values can be observed.

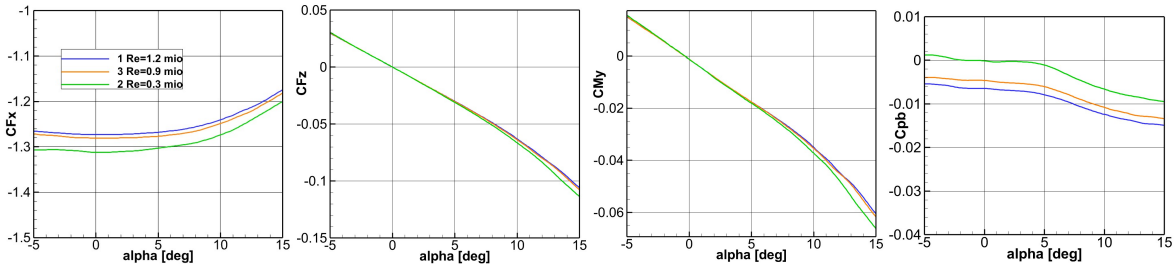

Fig. 12 Coefficients of the three test conditions at Ma=7 with deformed aeroshape, NT

Fig. 13 illustrates the aerodynamic coefficients as a function of AoA for the three test conditions at Mach 5.3. In contrast to the observed effect at Mach 7, at this Mach number, the Reynolds number has no visible influence on the axial force coefficient. Regarding normal force and pitching moment, an impact on the coefficients can only be observed for the lowest Reynolds number and above ~+3° AoA where the curves appear slightly shifted towards smaller absolute values. Similar to the observations at Mach 7, the base pressure decreases in absolute values when the Reynolds number is decreased.

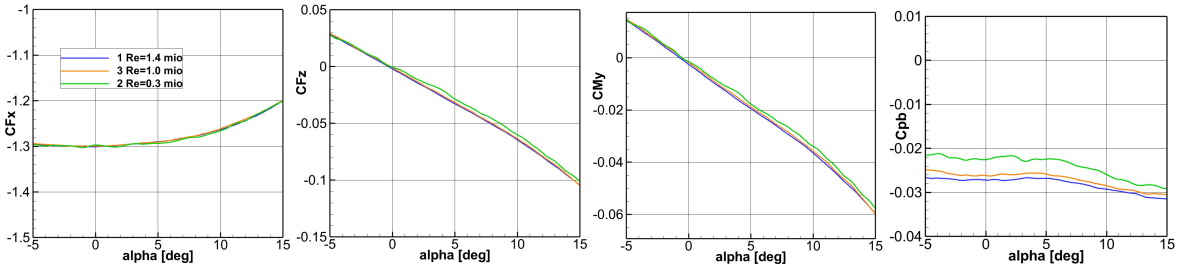

Fig. 13 Coefficients of the three test conditions at Ma=5.3 with deformed aeroshape, NT

To examine the impact of the turbulent boundary layer on the aerodynamic coefficients, the front surface is coated with carborundum with a grit size of 400 µm (Fig. 10). The effect of this treatment is illustrated in Fig. 14. The total value of the axial force coefficient increases in absolute values at small AoA, while the base pressure coefficient decreases in absolute values in the whole AoA range due to TT. This, coupled with observations from Schlieren images, indicates that the turbulent treatment might be effective. Additionally, an impact of TT on normal force and pitching moment coefficient is visible for angles of attack above ~+5°.

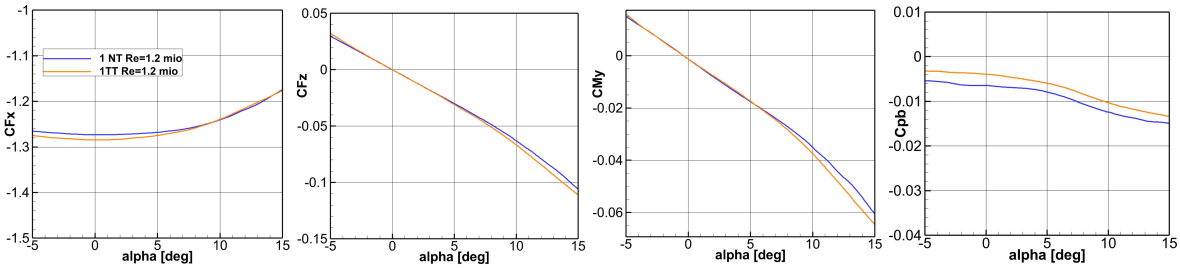

Fig. 14 Effect of tripping at Ma=7, Re=1.2 mio. with deformed aeroshape

Copyright © 2024 by author(s)

Further tests are performed to analyze the impact of the aeroshape deformation on the capsule's aerodynamic. The TMK model (described further below) with nondeformed aeroshape is tested in H2K at condition 2, equivalent dynamic pressure. Thereby, the aerodynamic coefficients for deformed and ondeformed aeroshape can be compared directly (Fig. 15). Regarding the axial force coefficient, there is nearly no impact of the shape deformation at Ma=7, but at Ma=5.3 the shape deformation leads to an absolute increase of the coefficient across the complete AoA range. Additionally, the shape deformation decreases the gradient of CMy at both Mach numbers.

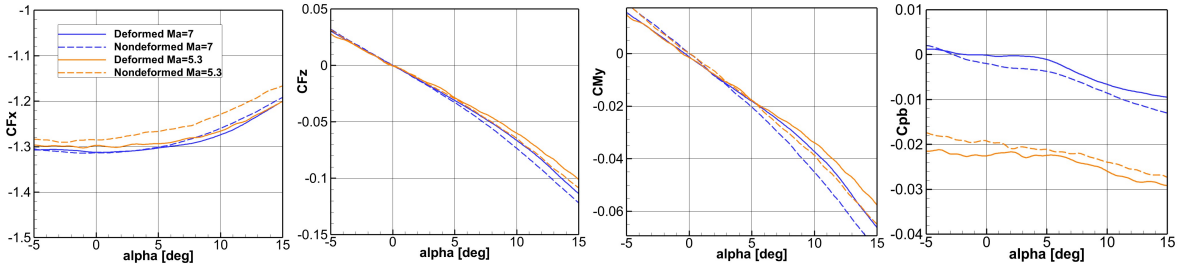

Fig. 15 Effect of the aeroshape on the coefficient at the test condition 2

Schlieren images captured at Mach 7, Reynolds number 1.2 mio (test condition 1) at AoA of 0° are presented in Fig. 16. The images at the left depict the smooth model (NT), while the images on the right display the TT. The top images were captured with a high-speed camera, while the bottom images were taken with a higher resolution camera. The bow shock wave outlines the contour of the IHS again. A slight difference in the flow structure between the two cases is visible in the area between bow shock and capsule surface.

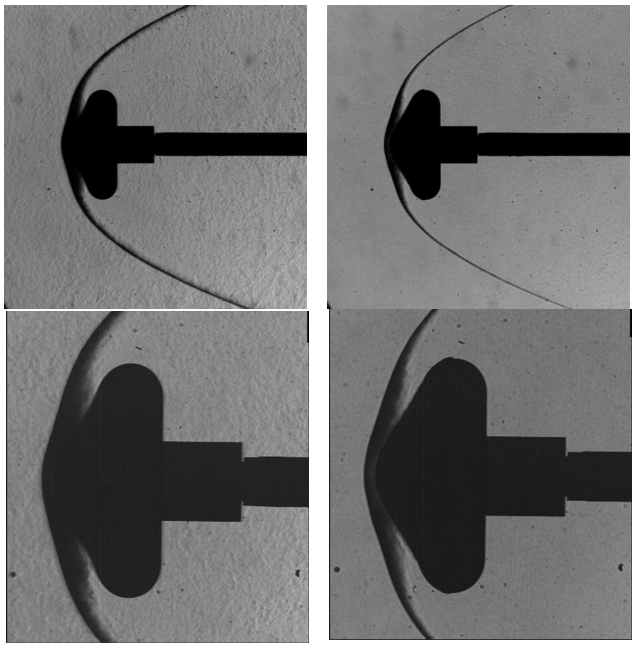

Fig. 16 Schlieren images captured at Mach 7, Re=1.2 mio; left: NT; right: TT; top: high-speed camera; bottom: higher resolution camera

4. EFESTO-2 in supersonic phase - TMK

4.1. Experimental setup

Trisonic wind tunnel cologne (TMK)

The facility TMK of DLR (see Fig. 17 on the left) is a tri-sonic blow down wind tunnel featuring a rectangular test section measuring 0.6m x 0.6m. Air from a 55 bar pressure reservoir passes through

Copyright © 2024 by author(s)

a storage heater and a settling chamber before being accelerated using an adjustable Laval nozzle. In the test section, the flow conditions remain constant. Downstream in the diffuser system, the flow is decelerated. Depending on Mach and Reynolds conditions, a maximum testing time of up to 60 seconds can be achieved (Esch, 1986).

Considering the allowable tunnel blockage, the Mach rhombus, balance loads, and the required Reynolds number, a model scale factor of 0.015 has been defined for the tests in TMK. Given that the flight dynamic pressure remains below 5kPa in the low Mach number range, the resulting shape deformation at such pressure rates is minimal. Therefore, the primary focus of the tests in TMK is to replicate the Reynolds number. The test range of TMK facility is depicted in Fig. 17 on the right.

The design of the model for TMK closely resembles that of H2K. Since this model is also utilized for dynamic stability testing, its CoG is intentionally positioned to match that of the original object. The model is equipped with an exchangeable central body to fit on balances with different diameter and also on a cross-pivot spring for dynamic tests.

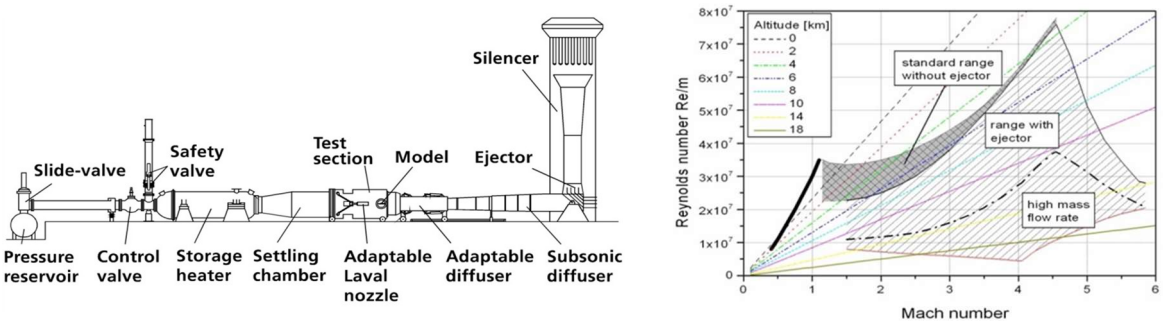

Fig. 17 TMK facility at DLR-Cologne (left); Performance map of TMK (right)

4.2. Wind tunnel model

Based on the results of the Fluid-Structure Interaction loop conducted, it has been found that no deformation occurs within the supersonic regime. Therefore, the wind tunnel tests in TMK are performed using the aeroshape in its nondeformed state.

The model sizing is crucial for a successful wind tunnel test in the supersonic regime. At one side, it is desirable to have a large model, so that more details of a flight object can be designed into a model and the test Re can be matched better to the flight Re. At the other side, a larger model means more blockage. This can lead to problems such as the tunnel will not start up for supersonic test, or the tunnel wall interference at sub- and transonic regime is so large that the flow in the tunnel is no more similar to that of the free flight. Because the load on a balance increases proportionally to the square of the model dimension, it's possible that no suitable balance may be available for a large model.

For capsule tests, previous experience indicates (Gawehn, 2022) (Gawehn, 2019) (Gawehn, 2019) that both the ratio of the sting diameter to the capsule diameter and the ratio of the sting length to the capsule diameter significantly influence the aerodynamic results. The optimal combination entails ensuring that the sting diameter does not exceed 18% of the capsule diameter, and its length is at least 3.55 times the capsule diameter. If enlarging the capsule diameter is not feasible, a longer sting becomes necessary.

After thorough consideration of the advantages and disadvantages, the model scale factor of 0.015 has been chosen. The nondeformed aeroshape is depicted on the left side in Fig. 18. It consists of a spherical nose, conical volume, annular volume and the central body.

Copyright © 2024 by author(s)

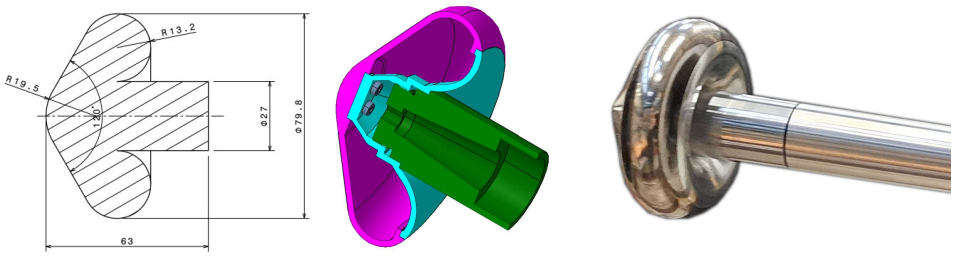

Fig. 18 The wind tunnel model of the nondeformed aeroshape for the test in TMK

Since dynamic aerodynamic tests with the nondeformed aeroshape will also be performed in TMK, it would be beneficial if the static model, or a portion of it, could be repurposed for the dynamic tests. The key requirement for the dynamic model is that its center of gravity (CoG) aligns with that of the real capsule. The CoG is situated approximately 48% behind the nose. To achieve this, the nose, conical section, and annular volume must be designed to be lightweight.

The same design procedure is employed as for the H2K model: initially, the aerodynamic load is estimated using CFD, and then the design is validated with FEM. The sectional view of the optimized wind tunnel model design is depicted in the middle of Fig. 18. It comprises the front and back shields, which feature a shell structure, the central body within which the balance is mounted. Constructed from high-strength aluminium alloy (EN AW 7022), both shields are meticulously manufactured. The front surface of the front shield is deliberately undersized by 30µm. Following mechanical manufacturing, the part undergoes a nickel coating process for protective purposes. The company's inspection protocol ensures a verified layer thickness of 31 µm.

The picture on the right in Fig. 18 displays the final mounted model, showcasing its surface finish quality. The model, including screws, weighs 222g.

4.3. Static aerodynamic measurements

The aerodynamic coefficients are determined using the internal six-component balance DLR-8904. Its structure closely resembles that of the balance DLR-8902, albeit with a larger diameter of 22mm and an expanded load range.

Before the test, the balance underwent calibration, with calibration points optimized according to the estimated loads from CFD simulation. Table 2 outlines the load range, maximum error, and the 95% uncertainty associated with each component. The maximum error and uncertainty values were derived from the calibration data. To calculate the uncertainty of the coefficients, the maximum error of the balance is utilized.

Due to the relatively small lift, the balance is mounted on the sting at a rolling angle of 90° around its axial axis. This configuration ensures that the lateral components are utilized for sensing the lift and the pitching moment, thereby enhancing accuracy.

Table 2 Technical data of balance DLR-8904

Component	Load range	Max. error	95% Uncertainty
Fx [N]	700	1.61	0.57
Fy [N]	500	0.38	0.12
Fz [N]	1250	0.57	0.22
Mx [Nm]	7	0.011	0.006
My [Nm]	625	0.031	0.012
Mz [Nm]	250	0.020	0.006

4.4. Flow visualizations

The schlieren setup for visualizing the flow field in TMK is similar to that utilized for H2K.

Copyright © 2024 by author(s)

4.5. Experimental test campaign

As outlined in section 2, the load on the IHS is minimal, resulting in practically no deformation during the supersonic phase. Consequently, the primary interest lies in replicating Mach number and Reynolds number in TMK.

TMK employs an adjustable Laval nozzle to set the Mach number in the test section. Through the utilization of an ejector, the static pressure can be manipulated, thereby allowing for adjustment of the Reynolds number independent of the Mach number. Additionally, its heat storage capacity enables the adjustment of the Reynolds number by altering temperature. However, this process is time-consuming and is primarily utilized to prevent condensation within the tunnel.

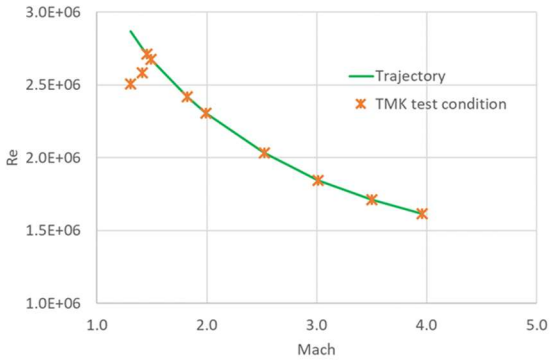

Fig. 19 Test condition for the test in TMK with the nondeformed aeroshape

4.6. Experimental results

Fig. 20 summarizes results from the tests in TMK with the smooth model (NT). It is important to note that the test conditions were determined to replicate the flight trajectory. Consequently, the effects presented here are a combination of the influences of Mach and Reynolds numbers.

From Mach 4 to 3, the axial force coefficient increases in absolute values with decreasing Mach number; whereas from Mach 2.5 to 1.5, it decreases in absolute values with decreasing Mach number. The base pressure decreases with Mach number monotonously, and satisfies approximately the experience relationship

$$C_{pb} \sim -\frac{1}{M^2}$$

Analyzing the normal force coefficient, it can be observed, that the curves for all Mach numbers are similar, but for Ma=1.5 the curve characteristic around the origin is different. At Ma=4, the pitching moment coefficient experiences a deviation from the other curves in the range 2°<AoA<15°.

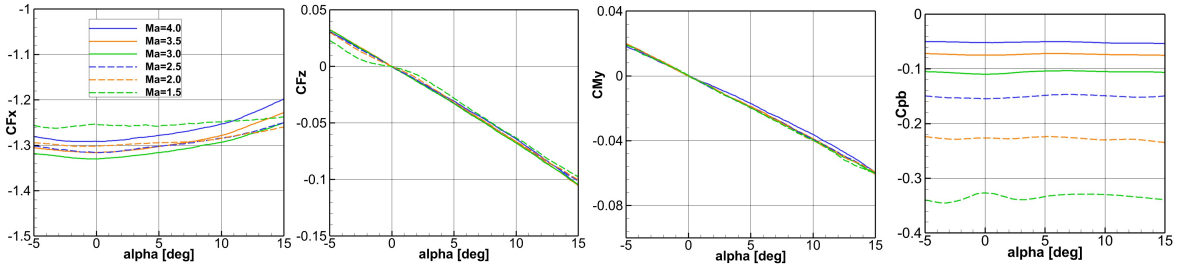

Fig. 20 Coefficients at various Mach numbers with nondeformed aeroshape, NT

The tripping effect is illustrated in Fig. 21. Here, the front surface is coated with carborundum with a grit size of 180μm. It's evident that TT results in increased absolute value of the axial force coefficient within AoA range from -5° to 15°, while simultaneously causing a decrease in the absolute value of the base pressure. Furthermore, the TT has no discernible impact on the normal force and pitching moment at lower AoA, but it elevates them at higher AoA.

Copyright © 2024 by author(s)

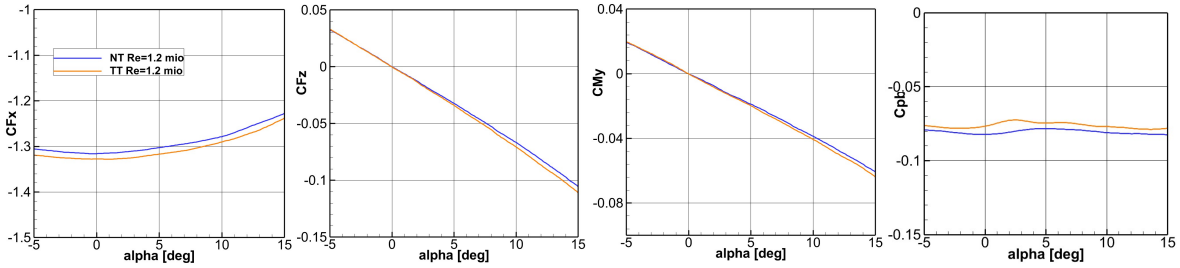

Fig. 21 Effect of tripping at Ma=3.5 with nondeformed aeroshape

Schlieren images captured at Mach 3.5 at AoA of 0° are presented in Fig. 22. The images at the left depict the smooth model (NT), while the images on the right display the TT. The top images were captured with a high-speed camera, while the bottom images were taken with the higher resolution camera. The wake behind the IHS is clearly visible in the images of the NT case whereby the shear layer is smeared in the TT case.

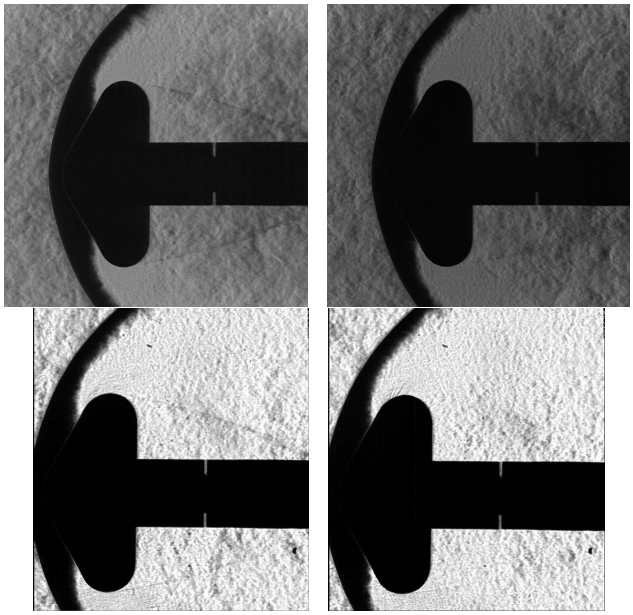

Fig. 22 Schlieren images captured at Mach 3.5 at AoA 0°, left: NT; right: TT; top: high-speed camera; bottom: higher resolution camera

4.7. Dynamic stability WTT in supersonic regime

The dynamic stability tests in TMK will be conducted using the free oscillation measurement technique (Gülhan, 2015). A critical component of this setup is the elastic cross-spring, as shown in Fig. 23. It is designed to provide the required rotational motion around the CoG. The stiffness of the spring is selected in such a way that the reduced frequency of the model inside the tunnel closely matches that experienced during free flight. Through a mechanism, the capsule is deflected and subsequently released to oscillate freely for a few seconds.

The cross-spring is instrumented with strain gages to record the deflection angle of the model. By analyzing the signals recorded during a wind tunnel test and applying calibration data along with model and wind tunnel parameters, the dynamic derivatives can be calculated.

Copyright © 2024 by author(s)

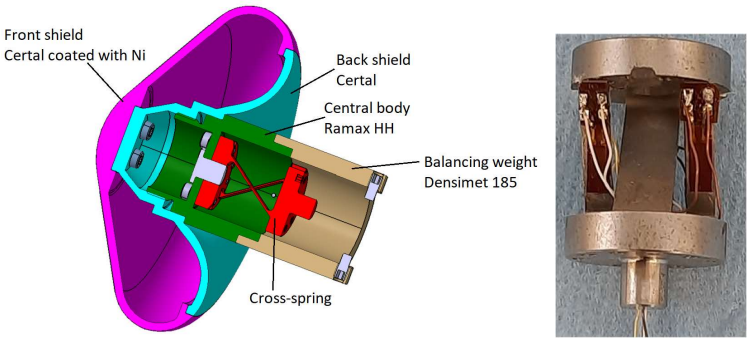

Fig. 23 View of dynamic wind tunnel model and the instrumented cross-spring

Dynamic testing is performed at conditions where the capsule experiences static aerodynamic stability. To evaluate this, the pitching moment coefficient is transferred from the reference point at the nose to the defined CoG of the capsule. The curves for Ma=4, 3 and 2 are depicted in Fig. 24, indicating static stability for all conditions as the gradient at the trim point is negative, even though relatively small. It can be observed that static stability increases when the Mach number decreases.

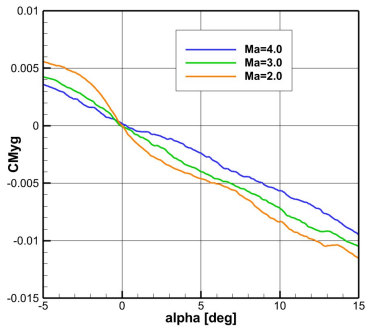

Fig. 24 Pitching moment coefficient with the reference point at CoG as a function of AoA

5. Conclusion

Evaluation of the IHS deformation influence on the aerodynamic coefficients and the wall heat flux is a key point of the design of the mission and the heat shield itself. To reach this objective, ground test campaigns and numerical rebuilding are necessary steps.

This paper presents the experimental characterization of the IHS in the hypersonic wind tunnel H2K and the supersonic wind tunnel TMK. An aerodynamic database was constructed from these wind tunnel tests. By varying the test conditions and model surface treatment, the influence of the Mach number, Reynolds number and the boundary layer on the coefficients was investigated. Analysis of the data reveals that the IHS remains aerodynamically stable in both hypersonic and supersonic regimes. The laminar or turbulent boundary layer affects the coefficients differently, with its influence dependent on the Mach and Reynolds numbers. Additionally, due to the deformation of the IHS, its stability decreases slightly.

These researches are conducted in the frame of the EFESTO-2 project. The EFESTO-2 project receives funding from the European Union under the Horizon Europe research and innovation programs, (grant agreement No.101081104). For further information, please visit the project website at: http://www.efesto-project.eu.

References

1. Daub, D. et al.: Experiments on aerothermoelastic fluid–structure interaction in hypersonic flow. In: Journal of Sound and Vibration, 2022/01/05, Available: https://doi.org/10.1016/j.jsv.2021.116714

Copyright © 2024 by author(s)

2. Dietlein, I. et al.: EFESTO-2: European Flexible Heat Shields Advanced TPS Design and Tests for Future In-Orbit Demonstration – 2. In: Aerospace Europe Conference 2023 – 10th EUCASS – 9th CEAS - Lausanne, Switzerland, 2023.

3. Esch, H.; Die 0.6-m x 0.6-m-Trisonische Meßstrecke (TMK) der DFVLR in Köln-Porz (Stand 1986). Mitteilung, DFVLR, Hauptabteilung Windkanäle, Köln, DRVLR-Mitt. 1986

4. Gardi, R. et al.: Design development and testing of the Inflatable Structure and its Demonstrator for the EFESTO project. In: 2nd International Conference on Flight Vehicles, Aerothermodynamics and Re-entry Missions & Engineering, Heilbronn, Germany, 2022.

5. Gawehn, T. et al.: Experimental Study on Static and Dynamic Stability of a Blunt Body Configuration. In: International Conference on Flight Vehicles, Aerothermodynamics and Re-entry Missions & Engineering (FAR 2019), Monopoli, Italy, 2019. [Online]. Available: https://elib.dlr.de/129437/

6. Gawehn, T. et al.: Impact of Shape Change on Capsule Aerodynamics and Shock-wave Boundary Layer Interaction. In: 2nd International Conference on Flight Vehicles, Aerothermodynamics and Re-entry Missions & Engineering (FAR), Heilbronn, Germany, 2022. [Online]. Available: https://elib.dlr.de/187173/

7. Gawehn, T. et al.: Capsule aerodynamics and shock-wave boundary layer interaction (SBLI) in supersonic and transonic flow. In: Experiments in Fluids, vol. 63, no. 3, p. 61, 2022/03/21 2022. [Online]. Available: https://elib.dlr.de/185835/.

8. Governale, G. et al.: Advanced European Re-Entry System Based on Inflatable Heat Shields EFESTO-2 project overview. In: 74th International Astronautical Congress (IAC), Baku, Azerbaijan, 2-6 October 2023.

9. Guidotti, G. et al.: The EFESTO project: Advanced European re-entry system based on inflatable heat shield. In: 2nd International Conference on Flight Vehicles, Aerothermodynamics and Re-entry Missions & Engineering - Heilbronn, Germany, 2022.

10. Guidotti, G. et al.: EFESTO 1 & 2: European Achievements And Expected Advancements In Inflatable Heat Shields For Mars And Earth Re-Entry Applications. In: 20th International Planetary Probe Workshop – Marseille, France, 2023.

11. Gülhan, A et al: Experimental Study on the Dynamic Stability of the IXV Configuration. In: 8th European Symposium on Aerothermodynamics for Space Vehicles, Lissabon, Portugal, March 2-6, 2015. [Online]. Available: https://elib.dlr.de/98422/

12. Langer, S. et al.: The dlr flow solver tau - status and recent algorithmic developments. In: 52nd Aerospace sciences meeting. National Harbor, Maryland, USA, 2018

13. Niezgodka, F.-J.: Der Hyperschallwindkanal H2K des DLR in Köln-Porz (Stand 2000). Windtunnel Department of Institute of Aerodynamic and Fluid Dynamics, Cologne, Germany (2002,in German)

14. Prevereaud, Y. et al.: Numerical aero-shape characterization of an Inflatable Heat Shield reentry vehicle in the EFESTO-2 project. In: Experimental aeroshape characterization of an Inflatable Heat Shield re-entry vehicle in the EFESTO-2 project.. In: 3rd International Conference on High-Speed Vehicle Science Technology (HiSST), Busan, Korea, 2024

15. Schleutker, T. et al.:Flexible TPS design and testing for advanced European re-entry system based on inflatable heat shield for EFESTO project. In: 2nd International Conference on Flight Vehicles, Aerothermodynamics and Re-entry Missions & Engineering - Heilbronn, Germany, 2022.

Copyright © 2024 by author(s)